

# A thin and soft optical tactile sensor for highly sensitive object perception

Yanchen Shen<sup>1</sup>, Kohei Tsuji<sup>1</sup>, Haruto Koizumi<sup>1</sup>, Jiseon Hong<sup>1</sup>, Tomoaki Niizuma<sup>2</sup>, Hiroyuki Kuwabara<sup>3</sup>, Hayato Ishida<sup>3</sup>, Jun Hiramitsu<sup>3</sup>, Mitsuhiro Mase<sup>3</sup>, and Satoshi Sunada<sup>2</sup>

<sup>1</sup>*Graduate School of Natural Science and Technology, Kanazawa University,  
Kakuma-machi, Kanazawa, Ishikawa, 920-1192, Japan*

<sup>1</sup>*Faculty of Mechanical Engineering, Institute of Science and Engineering,  
Kanazawa University, Kakuma-machi, Kanazawa, Ishikawa, 920-1192, Japan*

<sup>3</sup>*Hamamatsu Photonics K.K., 1126-1, Ichino, Chuo-ku, Hamamatsu, Shizuoka, 435-8558, Japan*

Tactile sensing is crucial in robotics and wearable devices for safe perception and interaction with the environment. Optical tactile sensors have emerged as promising solutions, as they are immune to electromagnetic interference and have high spatial resolution. However, existing optical approaches, particularly vision-based tactile sensors, rely on complex optical assemblies that involve lenses and cameras, resulting in bulky, rigid, and alignment-sensitive designs. In this study, we present a thin, compact, and soft optical tactile sensor featuring an alignment-free configuration. The soft optical sensor operates by capturing deformation-induced changes in speckle patterns generated within a soft silicone material, thereby enabling precise force measurements and texture recognition via machine learning. The experimental results show a root-mean-square error of 40 mN in the force measurement and a classification accuracy of 93.33% over nine classes of textured surfaces, including Mahjong tiles. The proposed speckle-based approach provides a compact, easily fabricated, and mechanically compliant platform that bridges optical sensing with flexible shape-adaptive architectures, thereby demonstrating its potential as a novel tactile-sensing paradigm for soft robotics and wearable haptic interfaces.

## I. INTRODUCTION

Mimicking the multiple mechanical sensing capabilities of the human skin has been a compelling goal in robotics and human–machine interaction. Soft tactile sensing systems aim to detect mechanical stimuli such as pressure, strain, temperature, and surface texture, enabling intelligent systems to interact safely and dexterously in complex environments [1–8].

In the early 1970s, researchers began exploring tactile sensing in artificial systems, developing pioneering devices such as prosthetic hands with rudimentary feedback and touch-sensitive computer interfaces [9, 10]. However, these seminal sensors were typically based on rigid materials and discrete transducers, providing limited spatial resolution and poor mechanical compliance. Over the last few decades, advances in flexible electronics and soft materials have led to significant progress in soft tactile sensors, enabling conformable skin-like devices capable of distributed and multimodal sensing [11, 12].

Tactile sensors used in soft systems can be broadly categorized into four types: piezoresistive, piezoelectric, capacitive, and optical, each with distinct operating principles and trade-offs. Piezoresistive sensors convert mechanical deformations into changes in resistance, providing straightforward readout circuitry and high sensitivity. However, they often suffer from hysteresis and drift [13–16]. Piezoelectric sensors use piezoelectric materials to generate electrical signals in response to dynamic pressure. Consequently, these sensors are suitable for vibration detection, but they are less effective for measuring static force [17, 18]. Capacitive sensors detect changes in electrode spacing or overlap. These sensors provide excellent sensitivity and low power consumption; however, they are susceptible to electromagnetic interference and require precise fabrication [19–21].

By contrast, optical tactile sensors offer unique advantages, including immunity to electromagnetic noise, high spatial resolution, and the potential for multiplexed sensing over long distances [8]. Various optical implementations have been reported, including those based on silica fibers [22–24], polymer fibers [25, 26], hydrogel [27–29], micro/nanofibers (MNFs) [30–32], and vision-based sensors [33]. Among these, vision-based tactile sensors (VBTSs) have emerged as a promising approach [34, 35]. By combining a deformable elastomer with a vision system, VBTSs can reconstruct high-resolution 3D surface topographies from contact-induced deformations, as exemplified by the well-known GelSight sensors [36–38]. Moreover, numerous other studies have proposed various novel approaches, such as ChromaTouch [39], BioTacTip [40], MagicTac [41], C-Sight [42], and ViTacTip [43].

Despite their high performances, VBTS systems have several limitations. They typically require high-resolution image sensors, precise optical alignment, and controlled illumination, making them sensitive to the focus distance and environmental conditions. Moreover, its integration into compact or highly flexible platforms is challenging due to the complex optical paths and rigid camera setups.

In this study, we present a thin, compact, and highly flexible optical tactile sensor featuring an alignment-free configuration. The sensing principle is based on speckle patterns generated within a soft transparent silicone elastomer.

Specifically, mechanical deformation of the elastomer is encoded into the speckle pattern via light scattering within the material [44, 45]. This optical interferometric technique enables the detection of minute optical path changes induced by subtle mechanical deformations, allowing accurate tactile sensing with a minimal number of components without requiring precise alignment. We demonstrate that the proposed tactile sensor achieves force sensing in the order of tens of millinewtons (mN), along with high-accuracy surface texture recognition, without relying on complex microstructures or intricate illumination schemes. This approach offers a simple, scalable, and geometrically versatile platform for next-generation optical tactile perception with promising applications in soft robotics and wearable systems.

## II. CONCEPT AND OPERATING PRINCIPLE

The sensor operation workflow is illustrated in Fig. 1(a). The proposed speckle-based tactile sensor comprises a transparent soft silicone elastomer as the sensing body, an optical fiber for delivering laser light to the elastomer, and a compact image sensor (e.g., a CMOS camera). Figure 1(b) shows the structure of the proposed sensor. Upon external contact, the mechanical deformation of the elastomer changes the position of the embedded scattering centers (e.g., glass microspheres), thereby modulating the internal light propagation paths. This modulation induces a reproducible transformation of the laser speckle pattern captured by the camera. Figure 1(c) illustrates representative speckle patterns collected under different contact conditions. A fixed area is cropped from the image, and the encoded tactile information is decoded from the cropped image using a decoding model.

Owing to the high refractive-index contrast between silicone and air, light rays striking the interface beyond the critical angle undergo total internal reflection, thereby confining most of the light within the elastomer. Reflective coatings are applied to the surfaces to enhance light confinement and sensing sensitivity, ensuring that light undergoes multiple passes through the scattering region. This extended propagation amplifies the interaction between light and mechanical deformation, increasing both the effective scattering depth and sensitivity.

The core transduction mechanism of the proposed sensor is based on encoding tactile information through optical scattering within the material. This mechanism is fundamentally different from those used in conventional VBTSSs, which typically rely on surface markers or structured illumination. The optical scattering-based approach offers several advantages: (i) high-precision and multimodal sensing enabled by its interferometric characteristics; (ii) elimination of the need for focusing lenses and precise optical alignment; (iii) reduced dependence on camera pixel resolution, enabling high-performance tactile sensing even with compact, low-resolution imaging hardware; and (iv) high geometric flexibility of the sensor architecture, allowing conformity to arbitrarily curved surfaces. For example, as shown in Fig. 1(d), the proposed sensor can be comfortably mounted on a human hand, demonstrating its adaptability to complex nonplanar surfaces.

### A. Feature Extraction and Classification Using Machine Learning

In this study, a lightweight convolutional neural network (CNN) was employed for the end-to-end classification of speckle patterns (Fig. 2). Prior to the network input, a central  $128 \times 128$ -pixel region was cropped from the raw image to focus on the region of deformation and reduce the computational load. The model processes single-channel input images and comprises three convolutional blocks followed by a fully connected classifier. Each block included a  $3 \times 3$  convolutional layer, followed by batch normalization, a ReLU activation function, and  $2 \times 2$  max pooling to reduce the spatial dimensions. After three downsampling operations, the feature maps are flattened and fed into a fully connected layer of 256 units, followed by batch normalization and ReLU activation. The final output layer decodes the sensing information, such as contact positions, contact force, or target classes, from the features. The network architecture was designed to trade-off between computational efficiency and classification accuracy. According to our estimation, the time of the inference was approximately 20.4 ms using a Raspberry Pi 5.

## III. DEVICE DESIGN AND FABRICATION

The sensor was fabricated using a two-component liquid rubber (Verde Co., Ltd., Deco Resina®super clear silicone). The base compound and curing agent were thoroughly mixed at a 10:1 weight ratio and poured into an acrylic mold. Optionally, glass beads (diameter: 0.2 mm) were embedded in the mixture prior to curing. The mixture was left to cure at room temperature for 24-h until it was fully solidified.

After demolding, a small incision was performed at the edge of the silicone rubber using a blade. A polarization-maintaining(PM) fiber (Thorlabs, PM630-HP, flat cleaved, 1 m) was inserted through this opening to enable side-

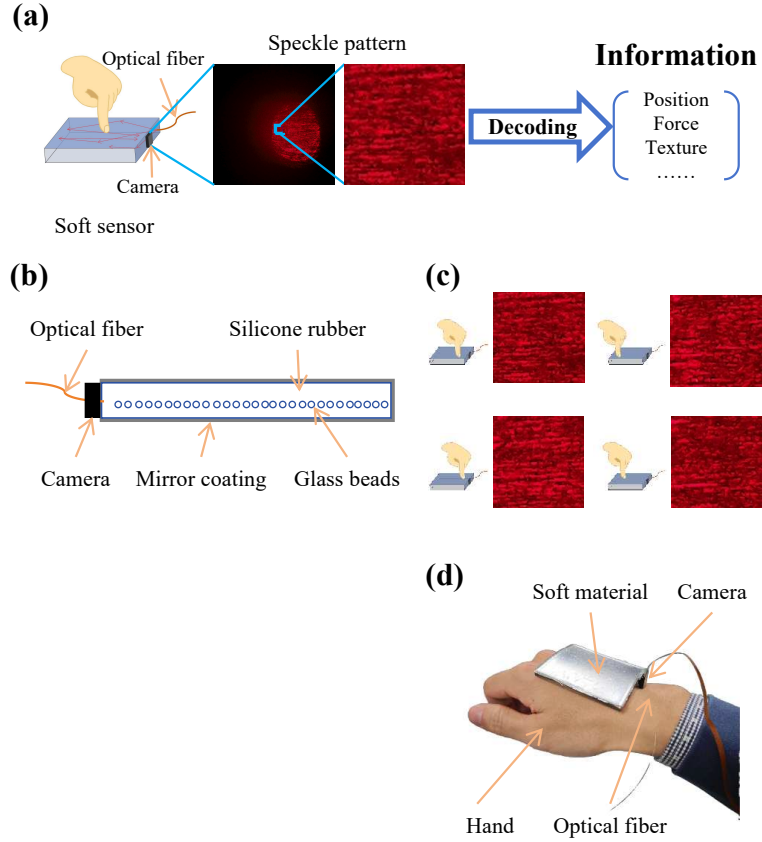


FIG. 1. (a) Schematic of the sensor operation. The camera captures the speckle pattern induced by laser illumination in the soft material. A central  $128 \times 128$  region is cropped and input to a decoding model (CNN) for tactile information extraction. (b) Structure of the proposed sensor. (c) Speckle patterns collected under different contact conditions. (d) Proposed sensor on a human hand.

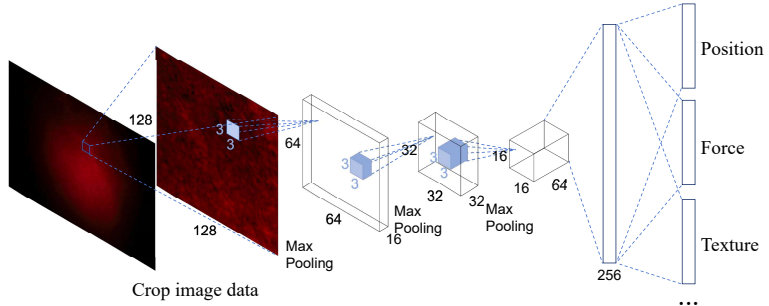


FIG. 2. Decoding model based on CNN.

coupled laser illumination. After applying the mirror coating to the surface, a layer of silicone was applied to protect the surface. Simultaneously, a small amount of uncured liquid silicone was applied around the fiber entry point and camera (ArduCam, OV5647 Spy Camera Module for Raspberry Pi) mounting area to securely fix both the fiber and camera modules. This secondary bonding step ensured mechanical stability and minimized the impact of relative displacement. After an additional 24-h curing period, the fabrication process was complete, yielding a monolithic, flexible tactile sensor ready for operation.

## IV. EXPERIMENTS

### A. Position recognition

To evaluate the spatial perception ability of the proposed sensor, we experimentally assessed the ability of the proposed approach to recognize positions across arbitrary shapes.

The experimental setup is shown in Fig. 3(a). A rectangular silicone rubber  $55 \times 61 \text{ mm}^2$  was manufactured as the sensing element. The thickness was 3 mm. A PM fiber laser (Civil Laser, 635 nm, spectral linewidth: 1 nm) was used as the light source. The resulting speckle patterns were captured using a compact camera coupled with a Raspberry Pi 4 Model B. The sensor was tested in two configurations on a flat surface, as shown in Fig. 3(b) and on a 3D-printed curved surface with a radius of curvature of 35 mm, as shown in Fig. 3(c).

To collect training and test datasets, a robotic arm (DOBOT, Magician) was used to simulate a human finger pressing at four predefined positions across the sensor's surface. Multiple force levels were applied at each position to investigate both the spatial location and robustness of the response. For each indentation event, a sequence of speckle images was recorded before and during contact.

The results of the position recognition on both flat and curved surfaces are presented in Fig. 3(d). Note that the predicted contact locations closely align with the ground truth across all tested positions, demonstrating high spatial accuracy in both configurations. These results demonstrate that the proposed tactile sensor maintains a high performance in different working environments, confirming its shape-adaptive capability and robustness.

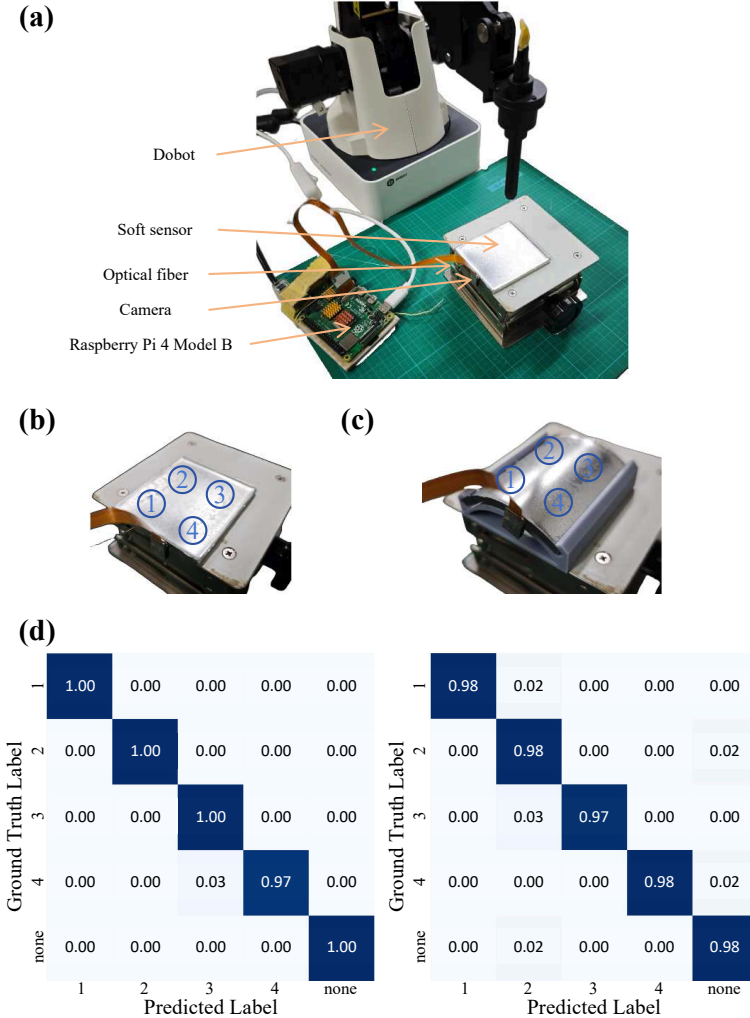


FIG. 3. (a) Experimental setup for position recognition. (b) Proposed sensor placement on a flat surface. (c) Proposed sensor placement on a curved surface. (d) Confusion matrix of the position recognition results. The left side shows the result placed on a flat surface; on the right is the result placed on a curved surface.

## B. Force measurement

We evaluated the ability of the proposed sensor to measure force. The experimental setup is shown in Fig. 4(a). The left side shows a fixed mount, where the proposed sensor is vertically installed. The right side shows a displacement controller capable of providing precise motion in both the vertical and lateral directions. A force sensor (CM085-5N, Minebea Mitsumi Inc.) and a metal rod were attached to the controller, which was used to apply controlled indentation forces onto the sensor surface. This system enabled accurate and repeatable control of the contact force, allowing for consistent tactile stimulation during the experiments.

Three different locations, labeled “A”, “B”, and “C”, were selected to test the force measurement capability, as shown in Fig. 4(b). The metal rod was driven by a displacement controller to apply controlled forces at the designated positions. After each displacement step, the force sensor readings and the corresponding speckle patterns were recorded. Each measurement was repeated three times to account for potential camera noise and ensure data consistency. The above procedure was repeated to collect training and test datasets.

The predicted forces were compared to the ground truth, as shown in Fig. 4(c). A strong correlation between the predicted and actual forces was observed across all three locations. This result indicates a consistent performance regardless of the contact location. The quantitative evaluation yielded mean absolute errors (MAEs) of 0.0291 N, 0.0260 N, and 0.0321 N, with corresponding root-mean-square errors (RMSEs) of 0.0391 N, 0.0339 N, and 0.0404 N for the three tested locations. Figure 4(d) shows the histograms of absolute errors. The errors exhibit a narrow distribution centered around zero, with most predictions falling within a small margin of error. The low error values and narrow variations across positions demonstrate high prediction accuracy and spatial uniformity in force estimation.

## C. Texture recognition

A more complex recognition task was conducted to demonstrate the texture recognition of the proposed tactile sensing approach. The experimental setup is shown in Fig. 5(a). To integrate the sensor with the robotic gripper, a soft tactile module with dimensions 28 mm  $\times$  28 mm  $\times$  6 mm was fabricated using the same materials and manufacturing process [Fig. 5(a)]. The sensor was mounted on the gripper and used to grasp various tiles, thereby enabling tactile interactions through controlled contact.

We utilized Mahjong tiles as the classification objects. Mahjong tiles (as shown in Fig. 5(b)) are small rectangular game pieces with engraved surface patterns and varying textures, which are typically fabricated of plastic or resin. Mahjong tiles were used as textured objects with subtle surface variations. Nine distinct classes were considered in this experiment: eight Mahjong tiles—namely, “White Dragon,” “Red Dragon,” “Green Dragon,” “One of Characters,” “One of Bamboos,” “Five of Circles,” “Six of Circles,” and “Seven of Circles”—as well as a ninth class representing the “no-contact” state. This expanded classification task tested the sensor’s ability to distinguish subtle differences in surface patterns and geometries. In total, 200 training and 40 test samples were collected from each class under consistent gripping conditions. The speckle patterns generated during contact were captured in real-time using a Raspberry Pi 4 Model B equipped with a camera module.

Figure 6 shows the results of the nine-class recognition task. In this experiment, we used speckle images cropped from the region labeled “A” in Fig. 7(a). The confusion matrix in Fig. 6 yielded an overall accuracy of 93.33%, demonstrating the sensor’s ability to distinguish fine surface textures based on speckle pattern evolution.

To further investigate the classification capability, we also used speckle images cropped from different regions labeled “B,” “C,” and “D” (see Fig. 7(a)). Classification accuracy varied depending on the selected region, achieving 86.11%, 91.67%, and 85.56%, respectively. While all regions maintained acceptable performance, the results indicate that performance depends on the local light path density or proximity to the illumination edge.

Furthermore, to assess data efficiency, we reduced the training set size per class from 200 to 50 samples while keeping the test set constant. Interestingly, as shown in Fig. 7(b), classification accuracy remained high at 90.56%. This result highlights the effectiveness of the speckle-based representation in capturing discriminative tactile features even with limited training data.

## V. DISCUSSION

Table I presents a comparison between the proposed sensor and representative VBTSSs. The proposed sensor offers several key advantages, including structural simplicity, a low profile, and shape adaptability.

Conventional VBTSSs typically require many components, including an illumination unit, camera, lenses, mounting holders, housing, and a soft elastomer. The required components total at least seven, as shown in Table I. The lenses must be precisely focused on the surface of the soft elastomer to capture deformation-induced visual changes. This

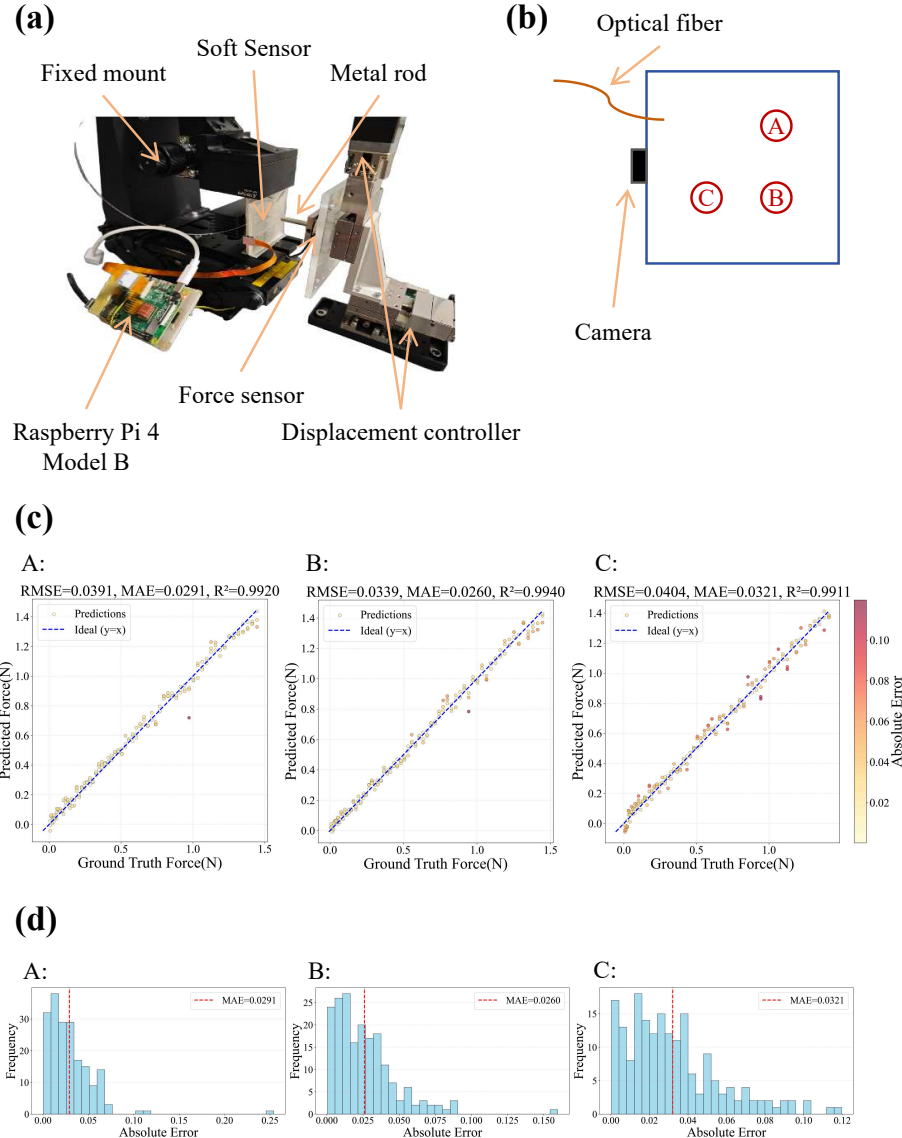


FIG. 4. (a) Experimental setup for force measurement. (b) Three locations (labeled “A”, “B”, and “C”) used for force measurement. (c) Scatter plots of the predicted forces versus the ground-truth values. RMSE and MAE denote the root-mean-square error and mean absolute error, respectively.  $R^2$  is the coefficient of determination. (d) Histograms of the absolute errors.

requirement necessitates rigid mechanical housings to maintain strict optical alignment and a fixed standoff distance between the lens and the sensing surface. Moreover, to enhance the visibility of subtle deformations, many designs incorporate elaborate internal structures, such as the dual-dome pigment layer in ChromaTouch [39] or the multi-material textured tip in BioTacTip [40]. These strategies are effective in improving signal contrast but significantly increase fabrication complexity and component count. Collectively, these factors lead to bulky, non-compliant systems that are ill-suited for integration into compact or highly flexible platforms.

In contrast, the proposed sensor was designed to operate without precise optical alignment and with a minimal number of components. This feature originates from the speckle-based sensing principle based on optical interference. While optical interferometric (speckle-based) approaches are highly sensitive, they also support large-area sensing through an alignment-free design and require only minimal core components: a laser source, a soft silicone medium, an optical fiber, and a compact camera. This simplified configuration significantly reduces fabrication complexity and overall system volume. Notably, the design does not require a large optical system to capture the full field of view of the sensor. As a result, the proposed sensor achieves a thin profile with an overall height of less than 3 mm, which is an order of magnitude thinner than that of conventional systems.

Moreover, the monolithic and flexible architecture enables the sensor to conform to arbitrary surfaces, offering

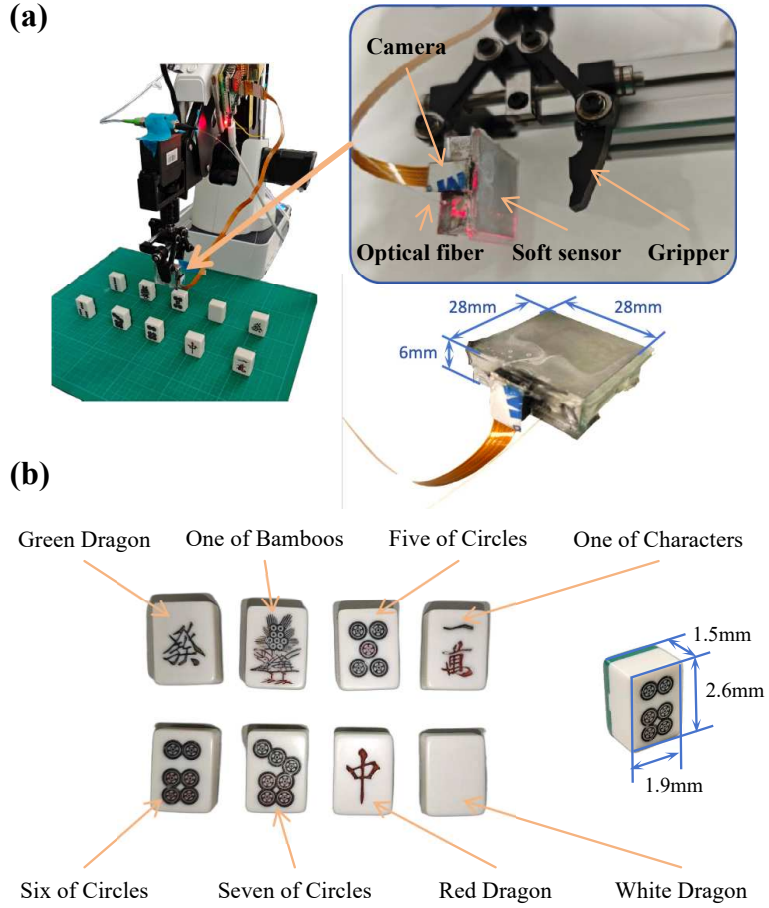


FIG. 5. (a) Experimental setup for Mahjong tile classification and the tactile sensor. The tactile sensor was designed to be mounted on a robotic gripper and used to grasp different tiles. (b) Mahjong tiles used in this experiment. The tiles are rigid cubes measuring 1.9, mm  $\times$  1.5, mm  $\times$  2.6, mm, with different patterns engraved on their surfaces.

superior mechanical compliance compared to rigid counterparts. In addition, the high sensitivity of the speckle pattern enabled precise force estimation, achieving a root-mean-square error (RMSE) of 0.04 N (40 mN), thereby demonstrating its capability for fine tactile perception.

## VI. CONCLUSION

In this study, we demonstrated a highly sensitive, speckle-based optical soft tactile sensor featuring a simple structure, low profile, and shape-adaptive capability. Experimental results showed that the proposed sensor can accurately recognize both contact location and applied force with a precision of 40 mN. The high accuracy achieved in tasks such as Mahjong tile classification highlights the sensor's sensitivity to fine surface features.

Future work includes optimizing the fabrication process, developing more efficient computational methods to improve system responsiveness, and exploring better integration strategies. These improvements will expand the applicability of the sensor to broader scenarios, including wearable devices, soft robotics, and human-machine interfaces.

## ACKNOWLEDGMENTS

This work was supported in part by the Japan Society for the Promotion of Science(JSPS) KAKENHI (Grant Nos. JP22K18792, JP22H05198, JP23K28157, JP25K22086), and Japan Science and Technology Agency(JST), Core

	One of Characters	0.00	0.00	0.00	0.00	0.00	0.00	0.00	0.00
One of Characters	1.00	0.00	0.00	0.00	0.00	0.00	0.00	0.00	0.00
One of Bamboos	0.00	0.95	0.00	0.03	0.00	0.00	0.00	0.03	0.00
Five of Circles	0.03	0.00	0.70	0.10	0.00	0.12	0.00	0.00	0.05
Six of Circles	0.00	0.03	0.00	0.97	0.00	0.00	0.00	0.00	0.00
Seven of Circles	0.00	0.00	0.00	0.00	0.97	0.00	0.00	0.03	0.00
Green Dragon	0.00	0.00	0.07	0.00	0.03	0.90	0.00	0.00	0.00
No-contact	0.00	0.00	0.00	0.00	0.00	0.00	1.00	0.00	0.00
Red Dragon	0.00	0.00	0.00	0.00	0.00	0.00	0.00	1.00	0.00
White Dragon	0.00	0.00	0.07	0.00	0.00	0.03	0.00	0.00	0.90
One of Characters	1.00	0.00	0.00	0.00	0.00	0.00	0.00	0.00	0.00

FIG. 6. Confusion matrix for the nine-class Mahjong tile classification task. The speckle images cropped from the region labeled “A” in Fig. 7(a) were used for classification. The overall accuracy was 93.33%.

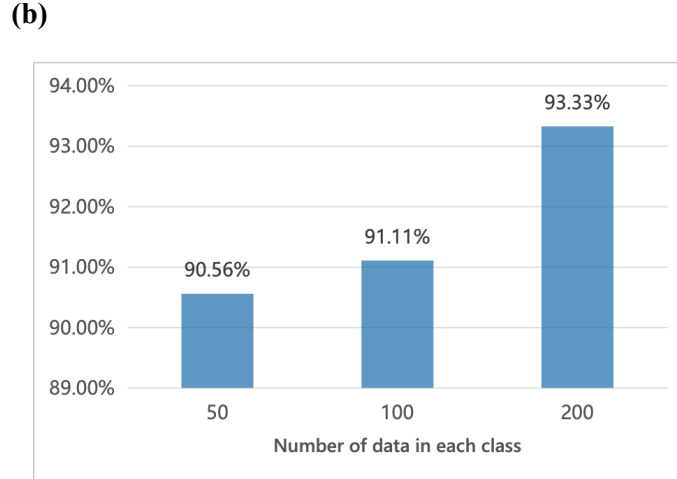
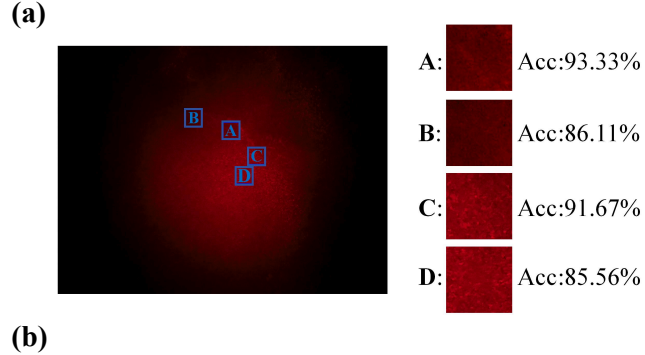


FIG. 7. (a) Cropped speckle images and the resulting classification accuracies. Four different image regions (labeled “A”, “B”, “C”, and “D”) were cropped from the original speckle image and used for the classification task. The classification accuracies were 93.33%, 86.11%, 91.67%, and 85.56%, respectively. (b) Classification accuracy as a function of the number of training samples per class.

TABLE I. Comparison between the proposed sensor and recent representative VBTS approaches. Components indicate the minimal number of components to build the system(including light source, soft materials, optical system, and etc). Prediction error indicates the force measurement error. Flexibility indicates whether the system can be flexibly adapted to different shapes.

Name	This work	ChromaTouch [39]	GelSlim 3.0 [38]
Principle	<b>Speckle based</b>	Color based	Colored shading based
Overall Height(mm)	<b>3 ~ 6</b>	-	20
Required Resolution	<b>128×128</b>	1600×1200	640×480
Prediction Error(N)	<b>0.04</b>	-	-
Components	<b>4</b>	8	10
Optical Alignment	<b>Not required</b>	Required	Required
Shape	Surface	Hemisphere	Flat
Flexibility	<b>yes</b>	no	no
Name	BioTacTip [40]	Digit360 [46]	ViTacTip [43]
Principle	Marker based	Reflective layer based	Intensity based
Overall Height(mm)	45	-	-
Required Resolution	1920×1080	-	1920×1080
Prediction Error(N)	0.1	0.001	0.04
Components	9	7	8
Optical Alignment	Required	Required	Required
Shape	Flat	Fingertip	Flat
Flexibility	no	no	no

Research for Evolutional Science and Technology(CREST) (Grant No. JPMJCR24R2).

---

[1] X. Wang, L. Dong, H. Zhang, R. Yu, C. Pan, and Z. L. Wang, Recent progress in electronic skin, *Advanced Science* **2**, 1500169 (2015).

[2] S. Tsuyoshi and S. Takao, Stretchable organic integrated circuits for large-area electronic skin surfaces, *MRS Bulletin* **37**, 236 (2012).

[3] E. Leogrande, M. Filosa, S. Ballanti, L. De Cicco, S. Mazzoleni, R. Ackerley, C. M. Oddo, and F. Dell’Olio, Electronic skin technologies: From hardware building blocks and tactile sensing to control algorithms and applications, *Sensors and Actuators Reports* **9**, 100312 (2025).

[4] M. Meribout, N. Abule Takele, O. Derege, N. Rifiki, M. El Khalil, V. Tiwari, and J. Zhong, Tactile sensors: A review, *Measurement* **238**, 115332 (2024).

[5] M. L. Hammock, A. Chortos, B. C.-K. Tee, J. B.-H. Tok, and Z. Bao, 25th anniversary article: The evolution of electronic skin (e-skin): A brief history, design considerations, and recent progress, *Advanced Materials* **25**, 5997 (2013).

[6] S. Jung, J. H. Kim, J. Kim, S. Choi, J. Lee, I. Park, T. Hyeon, and D.-H. Kim, Reverse-micelle-induced porous pressure-sensitive rubber for wearable human-machine interfaces, *Advanced Materials* **26**, 4825 (2014).

[7] J. C. Yang, J. Mun, S. Y. Kwon, S. Park, Z. Bao, and S. Park, Electronic skin: Recent progress and future prospects for skin-attachable devices for health monitoring, robotics, and prosthetics, *Advanced Materials* **31**, 1904765 (2019).

[8] N. Yao and S. Wang, Recent progress of optical tactile sensors: A review, *Optics and Laser Technology* **176**, 111040 (2024).

[9] J. Vedel and J. Roll, Response to pressure and vibration of slowly adapting cutaneous mechanoreceptors in the human foot, *Neuroscience Letters* **34**, 289 (1982).

[10] F. W. Clippinger, R. Avery, and B. R. Titus, A sensory feedback system for an upper-limb amputation prosthesis, *Bulletin of Prosthetics Research* , 247 (1974).

[11] G. Darlinski, U. Böttger, R. Waser, H. Klauk, M. Halik, U. Zschieschang, G. Schmid, and C. Dehm, Mechanical force sensors using organic thin-film transistors, *Journal of Applied Physics* **97**, 093708 (2005).

[12] I.-C. Cheng, S. Wagner, W. S. Wong, and A. Salleo, Overview of flexible electronics technology, in *Flexible Electronics: Materials and Applications* (Springer US, Boston, MA, 2009) pp. 1–28.

[13] S. Stassi, V. Cauda, G. Canavese, and C. F. Pirri, Flexible tactile sensing based on piezoresistive composites: A review, *Sensors* **14**, 5296 (2014).

[14] C.-L. Choong, M.-B. Shim, B.-S. Lee, S. Jeon, D.-S. Ko, T.-H. Kang, J. Bae, S. H. Lee, K.-E. Byun, J. Im, Y. J. Jeong, C. E. Park, J.-J. Park, and U.-I. Chung, Highly stretchable resistive pressure sensors using a conductive elastomeric composite on a micropyramid array, *Advanced Materials* **26**, 3451 (2014).

[15] R. Köiva, M. Zenker, C. Schürmann, R. Haschke, and H. J. Ritter, A highly sensitive 3d-shaped tactile sensor, in *2013 IEEE/ASME International Conference on Advanced Intelligent Mechatronics* (2013) pp. 1084–1089.

[16] Y. Ohmura, Y. Kuniyoshi, and A. Nagakubo, Conformable and scalable tactile sensor skin for curved surfaces, in *Proceedings*

2006 IEEE International Conference on Robotics and Automation, 2006. ICRA 2006. (2006) pp. 1348–1353.

[17] F. Qi, L. Xu, Y. He, H. Yan, and H. Liu, Pvdf-based flexible piezoelectric tactile sensors: Review, Crystal Research and Technology **58**, 2300119 (2023).

[18] C. Ryu, S. Hajra, M. Sahu, S. I. Jung, I. R. Jang, and H. J. Kim, Pvdf-bismuth titanate based self-powered flexible tactile sensor for biomechanical applications, Materials Letters **309**, 131308 (2022).

[19] H.-K. Lee, J. Chung, S.-I. Chang, and E. Yoon, Real-time measurement of the three-axis contact force distribution using a flexible capacitive polymer tactile sensor, Journal of Micromechanics and Microengineering **21**, 035010 (2011).

[20] D. J. Lipomi, M. Vosgueritchian, B. C.-K. Tee, S. L. Hellstrom, J. A. Lee, C. H. Fox, and Z. Bao, Skin-like pressure and strain sensors based on transparent elastic films of carbon nanotubes, Nature Nanotechnology **6**, 788 (2011).

[21] Y. Zang, F. Zhang, D. Huang, X. Gao, C.-a. Di, and D. Zhu, Flexible suspended gate organic thin-film transistors for ultra-sensitive pressure detection, Nature Communications **6**, 6269 (2015).

[22] M. Elsherif, A. E. Salih, M. G. Muñoz, F. Alam, B. AlQattan, D. S. Antonysamy, M. F. Zaki, A. K. Yetisen, S. Park, T. D. Wilkinson, and H. Butt, Optical fiber sensors: Working principle, applications, and limitations, Advanced Photonics Research **3**, 2100371 (2022).

[23] K. Kao and G. Hockham, Dielectric-fibre surface waveguides for optical frequencies, Proceedings of the Institution of Electrical Engineers **113**, 1151 (1966).

[24] M. Fajkus, J. Nedoma, R. Martinek, V. Vasinek, H. Nazeran, and P. Siska, A non-invasive multichannel hybrid fiber-optic sensor system for vital sign monitoring, Sensors **17**, 10.3390/s17010111 (2017).

[25] Y. Mizuno, A. Theodosiou, K. Kalli, S. Liehr, H. Lee, and K. Nakamura, Distributed polymer optical fiber sensors: a review and outlook, Photon. Res. **9**, 1719 (2021).

[26] H. Ma, A.-Y. Jen, and L. Dalton, Polymer-based optical waveguides: Materials, processing, and devices, Advanced Materials **14**, 1339 (2002).

[27] J. Guo, X. Liu, N. Jiang, A. K. Yetisen, H. Yuk, C. Yang, A. Khademhosseini, X. Zhao, and S.-H. Yun, Highly stretchable, strain sensing hydrogel optical fibers, Advanced Materials (Deerfield Beach, Fla.) **28**, 10244 (2016).

[28] C. Wang, B. Wu, S. Sun, and P. Wu, Interface deformable, thermally sensitive hydrogel–elastomer hybrid fiber for versatile underwater sensing, Advanced Materials Technologies **5**, 2000515 (2020).

[29] M. Elsherif, M. U. Hassan, A. K. Yetisen, and H. Butt, Hydrogel optical fibers for continuous glucose monitoring, Biosensors and Bioelectronics **137**, 25 (2019).

[30] L. Zhang, J. Pan, Z. Zhang, H. Wu, N. Yao, D. Cai, Y. Xu, J. Zhang, G. Sun, L. Wang, *et al.*, Ultrasensitive skin-like wearable optical sensors based on glass micro/nanofibers, Opto-Electronic Advances **3**, 190022 (2020).

[31] C. Jiang, Z. Zhang, J. Pan, Y. Wang, L. Zhang, and L. Tong, Finger-skin-inspired flexible optical sensor for force sensing and slip detection in robotic grasping, Advanced Materials Technologies **6**, 2100285 (2021).

[32] J. Pan, Z. Zhang, C. Jiang, L. Zhang, and L. Tong, A multifunctional skin-like wearable optical sensor based on an optical micro-/nanofibre, *anoscale* **12**, 17538 (2020).

[33] K. Sato, K. Kamiyama, N. Kawakami, and S. Tachi, Finger-shaped gelforce: Sensor for measuring surface traction fields for robotic hand, IEEE Transactions on Haptics **3**, 37 (2010).

[34] Y.-H. Xin, K.-M. Hu, R.-J. Xiang, Y.-L. Gao, J.-F. Zhou, G. Meng, and W.-M. Zhang, Vision-based tactile sensing: From performance parameters to device design, Applied Physics Reviews **12**, 021312 (2025).

[35] H. Li, Y. Lin, C. Lu, M. Yang, E. Psomopoulou, and N. F. Lepora, Classification of vision-based tactile sensors: A review, IEEE Sensors Journal **25**, 35672 (2025).

[36] W. Yuan, S. Dong, and E. H. Adelson, Gelsight: High-resolution robot tactile sensors for estimating geometry and force, Sensors **17** (2017).

[37] E. Donlon, S. Dong, M. Liu, J. Li, E. Adelson, and A. Rodriguez, Gelslim: A high-resolution, compact, robust, and calibrated tactile-sensing finger, in *2018 IEEE/RSJ International Conference on Intelligent Robots and Systems (IROS)* (2018) pp. 1927–1934.

[38] I. H. Taylor, S. Dong, and A. Rodriguez, Gelslim 3.0: High-resolution measurement of shape, force and slip in a compact tactile-sensing finger, in *2022 International Conference on Robotics and Automation (ICRA)* (2022) pp. 10781–10787.

[39] R. B. Scharff, D.-J. Boonstra, L. Willemet, X. Lin, and M. Wiertlewski, Rapid manufacturing of color-based hemispherical soft tactile fingertips, in *2022 IEEE 5th international conference on soft robotics (RoboSoft)* (IEEE, 2022) pp. 896–902.

[40] H. Li, S. Nam, Z. Lu, C. Yang, E. Psomopoulou, and N. F. Lepora, Biotactip: A soft biomimetic optical tactile sensor for efficient 3d contact localization and 3d force estimation, IEEE Robotics and Automation Letters **9**, 5314 (2024).

[41] W. Fan, H. Li, and D. Zhang, Magictac: A novel high-resolution 3d multi-layer grid-based tactile sensor, in *2024 IEEE International Conference on Robotics and Automation (ICRA)* (IEEE, 2024) pp. 388–394.

[42] W. Fan, H. Li, Y. Xing, and D. Zhang, Design and evaluation of a rapid monolithic manufacturing technique for a novel vision-based tactile sensor: C-sight, Sensors **24** (2024).

[43] W. Fan, H. Li, W. Si, S. Luo, N. Lepora, and D. Zhang, Vitactip: Design and verification of a novel biomimetic physical vision-tactile fusion sensor, in *2024 IEEE International Conference on Robotics and Automation (ICRA)* (IEEE, 2024) pp. 1056–1062.

[44] S. Shimadera, K. Kitagawa, K. Sagehashi, Y. Miyajima, T. Niiyama, and S. Sunada, Speckle-based high-resolution multi-modal soft sensing, Scientific Reports **12**, 13096 (2022).

[45] K. Kitagawa, K. Tsuji, K. Sagehashi, T. Niiyama, and S. Sunada, Optical hyperdimensional soft sensing: speckle-based touch interface and tactile sensor, Opt. Express **32**, 3209 (2024).

[46] M. Lambeta, T. Wu, A. Sengul, V. R. Most, N. Black, K. Sawyer, R. Mercado, H. Qi, A. Sohn, B. Taylor, *et al.*, Digitizing touch with an artificial multimodal fingertip, arXiv preprint arXiv:2411.02479 (2024).